Incident beam effects in medium-energy backscattered electron diffraction

S. A. Chambers,* I. M. Vitomirov, and J. H. Weaver
Department of Chemical Engineering and Materials Science, University of Minnesota, Minneapolis, Minnesota 55455
(Received 5 January 1987)

We have examined the angular distributions of medium-energy (500–1500 eV) elastically backscattered electrons from bulk Cu(001) and Ni(001) crystals and from pseudomorphic Cu on Ni(001). The observed diffraction features are largely governed by forward scattering of the outgoing electrons, and incoming beam scattering appears to play a relatively minor role. This conclusion is reached by comparing these angular distributions with theoretical angular distributions, and with those obtained via angle-resolved Auger electron and x-ray photoelectron diffraction spectroscopies involving electrons of comparable kinetic energies. We find that the three experimental techniques yield very similar results, indicating that incident beam effects and the mode of excitation play a minor role. In the calculations, we have both included and neglected incident beam diffraction. By including incoming beam diffraction, we have for simplicity ignored the phase relationship between incoming and outgoing beams. The result is that inclusion of incoming beam scattering does not particularly improve the level of agreement between theory and experiment relative to calculations which neglect incoming beam diffraction. Moreover, the level of agreement between experiment and theory is quite good for the simpler theory which only treats outgoing electron scattering. Finally, we find that azimuthal-angle medium-energy backscattered electron diffraction scans for pseudomorphic Cu/Ni(001) are not as sensitive to elastic overlayer strain as are polar-angle scans. The latter measurement provides a highly sensitive method of measuring strain which is quite straightforward to interpret.

In two previous papers we demonstrated that high-energy Auger electron diffraction[1](AED) and medium-energy backscattered electron diffraction[2](MEED) could be used to measure elastic strain in ultrathin pseudomorphic overlayers of Cu on Ni(001). The critical measurement was shown to be a polar-angle scan of either Cu $L_{2,3}M_{4,5}M_{4,5}$ Auger intensity (916 eV) or elastically backscattered intensity at 1 keV in the (010) azimuthal plane. Both measurements exhibited an upward shift of 1.2°–1.5° in the polar angle at which the forward-scattering-induced peak along [101] occurred, indicative of tetragonal distortion in the overlayer accompanying compressive strain in the interface plane.

The angular scans described above were chosen to show strain-induced changes in a most obvious way—a shift in the [101] diffraction peak. Moreover, the polar-angle distributions involving both 1000-eV backscattered electrons and high-energy Auger electrons were very well described by a straightforward kinematical or single-scattering cluster formalism in which only outgoing beam scattering was treated.[3] This rather surprising result was rationalized by pointing out that the experimental geometry was such that peaks associated with incoming and outgoing beam forward scattering nearly overlap, causing the two effects to reinforce one another.[2] In this paper, we present results over a wide range of angles and electron energies to demonstrate that the observed modulation in MEED measurements is more generally dominated by outgoing beam diffraction and is, therefore, very well accounted for in terms of simple kinematical scattering of the backscattered beam. We also show that inclusion of incoming beam scattering at a simple kinematical level does not significantly improve agreement with experiment. Possible reasons for this result are given. Finally, we show that azimuthal scans of MEED intensity at various polar angles are relatively insensitive to tetragonal distortion in a 12-Å (six monolayers) pseudomorphic Cu overlayer on Ni(001), compared to polar scans in the (010) azimuthal plane.

In Fig. 1 we show azimuthal MEED, high-energy Auger electron diffraction, and high-energy x-ray photoelectron diffraction (XPD) scans at a polar angle (θ) of 45° relative to the Cu or Ni (001) surface plane for a wide variety of electron kinetic energies. This angular scan includes scattering of the outgoing electrons along [101] ($\phi=0°$) and [011] ($\phi=90°$), and the incident beam sweeps a cone of half-angle 3° centered on [001] in the MEED and AED experiments. The electron kinetic energies in the MEED scans were chosen to match those of the Ni *LMM* Auger series ($L_{2,3}M_{2,3}M_{2,3}$ at 707 eV, $L_{2,3}M_{2,3}M_{4,5}$ at 772 eV, and $L_{2,3}M_{4,5}M_{4,5}$ at 844 eV), one of the Cu *LMM* Auger lines ($L_{2,3}M_{4,5}M_{4,5}$ at 916 eV), and the kinetic energies of Cu $2p_{3/2}$ and $3p$ x-ray photoelectrons at an x-ray energy of 1486 eV (554 and 1410 eV, respectively). Furthermore, incident beam diffraction is expected to be essentially constant, inasmuch as the direction of incidence is nearly coincident with [001] throughout the scan. These choices of kinetic energy then allow direct comparison of MEED results with Ni(001) *LMM* Auger angular distributions and with analogous x-ray photoelectron diffraction scans for Cu(001) by Trehan and Fadley.[4] In describing both XPD and AED phenomena, it is assumed that scattering of the exciting beam can be ignored, allowing the ob-

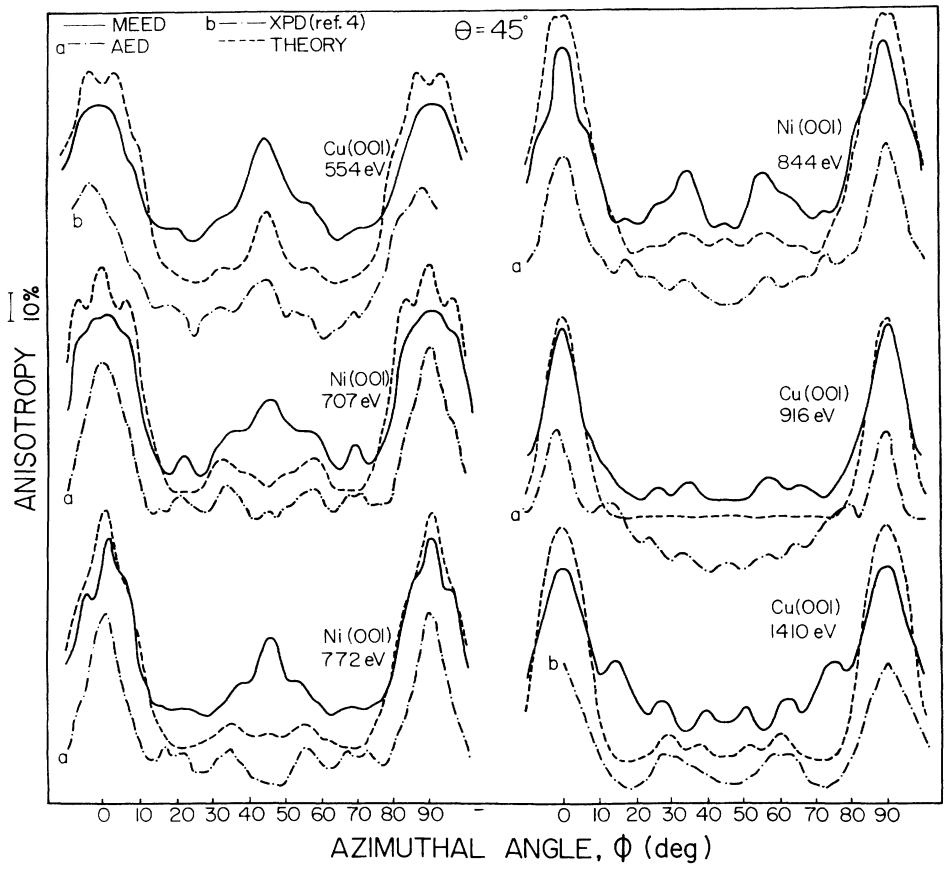

FIG. 1. Azimuthal scans of medium-energy electron diffraction (MEED), Auger electron diffraction (AED), and x-ray photoelectron diffraction (XPD) intensities at a polar angle (θ) of 45° for electron kinetic energies ranging from 554 to 1410 eV for Cu(001) and Ni(001). The angular resolution of the MEED and AED scans was $\Delta\theta\Delta\phi = 2° \times 4°$. The XPD scans (Ref. 4) at 554 and 1610 eV were obtained with $\Delta\theta = 1.2°$ and 7.4°, respectively. Also included are plots of Eq. (1) employing angular averaging corresponding to the instrumental resolution of the MEED-AED spectrometer. $\phi = 0°$ corresponds to [101] and $\phi = 90°$ corresponds to [011].

served intensity modulation to be connected with outgoing electron scattering and interference. The validity of this assumption is confirmed by the success with which experimental results can be accounted for using a single-scattering cluster model which treats diffraction of the Auger and photoelectrons and ignores incident beam effects.[1,3-6] Therefore, scanning from $\phi = 0°$ to $\phi = 90°$ at $\theta = 45°$ constitutes a good way to find out if MEED and AED or XPD yield similar results in a geometry that minimizes incident beam effects.

In comparing the different scans in Fig. 1, it is clear that there are strong similarities between the MEED, AED, and XPD diffraction peaks along [101] and [011] at each kinetic energy ($\phi = 0°$ and 90°, respectively). There is, in addition, a decrease in peak width as kinetic energy increases, in keeping with the dependence of the atomic scattering factor on energy.[7] These results demonstrate that intensity maxima along close-packed directions are determined largely by forward scattering of the outgoing electron, with the mode of excitation playing a negligible role. However, this does not appear to be consistently the case for the fine structure between $\phi \cong 10°$ and 80°, in which differences appear between the MEED and AED or XPD profiles at a given energy, and between the MEED profiles obtained at different energies. For instance, while there are strong similarities between the MEED and AED or XPD fine structure at 554, 844, and 916 eV, there are notable differences at 707, 772, and 1410 eV. Likewise, at 707 and 772 eV, there is a major peak at $\phi = 45°$ in the MEED scan which is not seen in the AED scans. At 1410 eV, the MEED profile shows additional fine structure at $\phi \cong 15°$, 40°, 50°, and 75° not seen in the XPD scan. Furthermore, looking at the AED scans at 707, 772, and 844 eV, there are only very minor changes in the fine structure over this energy range. (All three profiles were obtained with an incident beam energy of 5 keV.) However, the MEED fine-structure changes considerably over the same energy range. Thus, it does not appear that differences in outgoing electron scattering brought about by changes in the electron wavelength (a 9% decrease from 707 to 844 eV) are responsible for the differences in the MEED fine structure with energy. Although this angular scan should be dominated by outgoing beam diffraction, the differences between MEED and AED or XPD data noted above suggest that incident beam effects may play a minor role in producing the observed anisotro-

pies, even though the primary beam is nearly aligned with [001]. In order to try to account for differences in fine structure seen in Fig. 1, we have performed diffraction calculations in which incoming beam scattering is treated in a manner analogous to that of outgoing beam scattering, as described below.

A complete theory of MEED in a backscattering geometry such as we have employed would, of necessity, be dynamical in nature. In order to avoid the complexities of such calculations, we have instead broken the problem down into two independent kinematical problems, one for primary beam diffraction and one for backscattered beam diffraction. At this level of approximation, incident beam diffraction can be thought of as acting to locally modify the backscattering cross section directly through modulation of the incident beam flux at a particular ion core. Ignoring the phase relationship between incident and outgoing beams, we can then write the total backscattered flux at the detector, $I(\theta,\phi)$, as

$$I(\theta,\phi) \propto \sum_l I_{\rm in}^{(l)}(\mathbf{k}) I_{\rm out}^{(l)}(\mathbf{k}') \ , \tag{1}$$

where $I_{\rm in}^{(l)}(\mathbf{k})$ is the incident beam flux at the lth atom in the crystal and $I_{\rm out}^{(l)}(\mathbf{k}')$ is the corresponding outgoing beam flux for a constant incident beam intensity. The sum is over atoms which are in unique symmetry sites in each layer. The vectors $\mathbf{k}$ and $\mathbf{k}'$ differ only in their direction in that primary electrons must backscatter through an angle of 138° to be energy analyzed in our spectrometer.

The incoming beam intensity for the lth backscatterer can be written as

$$I_{\rm in}^{(l)}(\mathbf{k}) \propto \left| \exp\left[-\frac{L_l}{2\lambda}\right] + \sum_k \frac{|f_k(\theta_k)|}{r_k} W_k \exp\left[-\frac{L_k+r_k}{2\lambda}\right] \exp\{i[\,|k|\, r_k(1-\cos\theta_k)+\psi_k(\theta_k)]\} \right|^2 + \sum_k \frac{|f_k(\theta_k)|^2}{r_k^2} \exp\left[-\frac{L_k+r_k}{\lambda}\right](1-W_k^2) \tag{2}$$

and the outgoing beam intensity is

$$I_{\rm out}^{(l)}(\mathbf{k}') \propto \left| \exp\left[-\frac{L_l'}{2\lambda}\right] + \sum_j \frac{|f_j(\theta_j')|}{r_j'} W_j \exp\left[-\frac{r_j'+L_j'}{2\lambda}\right] \exp\{i[\,|k'|\, r_j'(1-\cos\theta')+\psi_j(\theta_j')]\} \right|^2 + \sum_j \frac{|f_j(\theta_j')|^2}{r_j'^2} \exp\left[-\frac{r_j'+L_j'}{\lambda}\right](1-W_j^2) \ . \tag{3}$$

The relevant geometric parameters are shown in Fig. 2. The incident intensity at the lth backscatterer is given by the superposition of an incident unscattered plane wave with momentum $\mathbf{k}$ and waves which have scattered once from all atoms in the cluster, and arrive at atom l having undergone path-length changes and phase differences of $r_k(1-\cos\theta_k)$ and $\psi_k(\theta_k)$, respectively. The amplitude of the unscattered incident plane wave will have decayed by an amount equal to $\exp(-L_l/2\lambda)$ by the time it reaches the lth backscatterer, where λ is the inelastic mean-free path. Lattice vibrations are accounted for in the usual way by a Debye-Waller factor W_k. A critical assumption in this part of the development is the use of asymptotic forms of the wave functions for scattered waves in the vicinity of the lth backscatterer. While perfectly valid for outgoing electron diffraction at the detector point, this simplifying assumption is clearly an approximation for distances of the order of a few angstroms.

Diffraction of the outgoing electron is treated in the same way as in AED or XPD. The "primary" wave emitted from the lth backscatterer is assumed to be isotropic, which is essentially correct for all directions except within $\cong \pm 40°$ of the incident direction (the forward-scattering region). Only those electrons which backscatter through an angle of $\cong 138 \pm 20°$ will contribute significantly to the observed diffraction intensity, and such backscattering will be very nearly isotropic. As with incoming beam diffraction, interference of the outgoing electron is dominated by the path-length differences $[r_j'(1-\cos\theta_j')]$ and phase shifts $[\psi_j(\theta_j')]$ associated with scattering at each other atom in the cluster. Refraction is taken into account for both beams by treating the solid-vacuum inter-

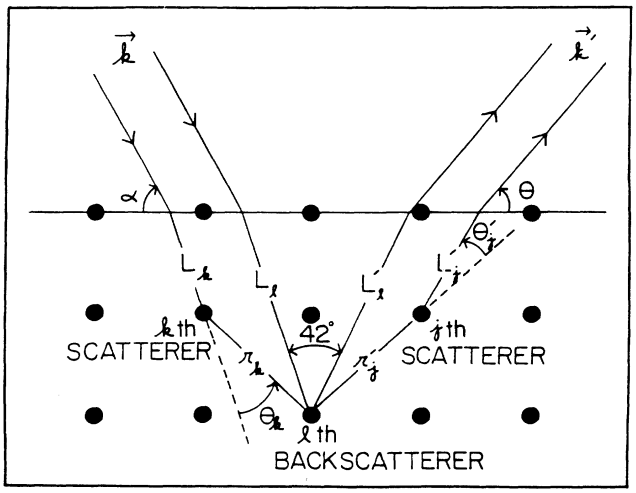

FIG. 2. Geometric parameters used in the formulation of Eqs. (1)–(3) as discussed in the text. The scattering angle in the MEED-AED spectrometer is fixed at 138°.

face as a potential step of height V_0 (the inner potential of the solid)[3] and results in a slight direction change at the surface, which is shown in an exaggerated form in Fig. 2.

The atomic scattering factors used in Eqs. (2) and (3) were taken from tabulated values based on free-atom scattering of incident plane waves,[8,9] and were subsequently reduced by a factor of 2 prior to use in Eqs. (2) and (3). This empirical reduction is intended to offset spherical-wave effects and multiple scattering which are neglected in the present calculations. Spherical-wave effects have recently been included in forward and backscattering photoelectron diffraction[10,11] and surface extended x-ray-absorption fine-structure[12] (SEXAFS) calculation schemes. The SEXAFS curved-wave correction is particularly simple and easily incorporated into the MEED-AED calculation. Assuming s-wave Auger emission in AED and isotropic backscattering in the MEED experiment, the atomic scattering strength a distance R from the Auger emitter or backscatterer is given by

$$f(\theta,R)=\frac{1}{|k|}\sum_l (2l+1)\sin\delta_l \exp(i\delta_l)P_l(\cos\theta) \times\left[1+\frac{[l(l+1)]}{2|k|^2R^2}\right]^{1/2} \times\exp\left[\frac{i[l(l+1)]}{2|k|R}\right], \quad (4)$$

where θ is the scattering angle, δ_l is the scattering phase shift for a partial wave with angular momentum l, $P_l(\cos\theta)$ is a Legendre polynomial of order l, and k is the electron wave vector. We have evaluated Eq. (4) with phase shifts generated for plane waves interacting with a muffin-tin potential appropriate for Ni using the program MUFPOT,[13] and have then used the resulting scattering factors in Eq. (3) (outgoing beam diffraction only) to predict the azimuthal-angle dependence at $\theta=45°$ of Ni $L_{2,3}M_{4,5}M_{4,5}$ Auger and 844-eV elastic peak intensity in Ni(001). The results of these calculations, as well as those in which free-atom–plane-wave (FA-PW) scattering factors and muffin-tin–plane-wave (MT-PW) scattering factors were used are shown in Fig. 3. The intent here is to assess the changes in theoretical angular distributions brought about by the inclusion of solid-state and curved-wave effects relative to calculations in which free-atom–plane-wave scattering factors are used.

As has been shown by Sagurton *et al.*,[10] inclusion of spherical-wave effects, using the correction proposed by Rehr *et al.*[12] [essentially Eq. (4) with curved-wave corrections appropriate to a p wave rather than an s wave] effectively does away with the empirical reduction in f needed when plane-wave scattering is assumed. As Fig. 3 shows, the use of muffin-tin potential phase shifts with either incident plane waves (MT-PW) or spherical waves (MT-SW) does bring the intensity of calculated forward-scattering-induced features ([101] and [011]) into closer agreement with experiment, without the reduction in f seemingly necessary in the FA-PW approach. The maximum anisotropy for the MT-PW and MT-SW calculations without any reduction in scattering strength is 83% and 81%, respectively, whereas that for the FA-PW calculation is 86% with a factor-of-2 reduction in the scattering factors. The use of MT phase shifts alone partially eliminates spherical-wave effects because MT potentials typically fall off more rapidly with distance than analogous FA potentials. Therefore, the small-atom approximation is more appropriate for a MT potential than for a FA potential.

One undesirable side effect of using a MT potential and a SW correction is the broadening of forward-scattering peaks along low-index directions and the addition of fine structure to such peaks, neither of which are seen in the experimental data. As Fig. 3 shows, the

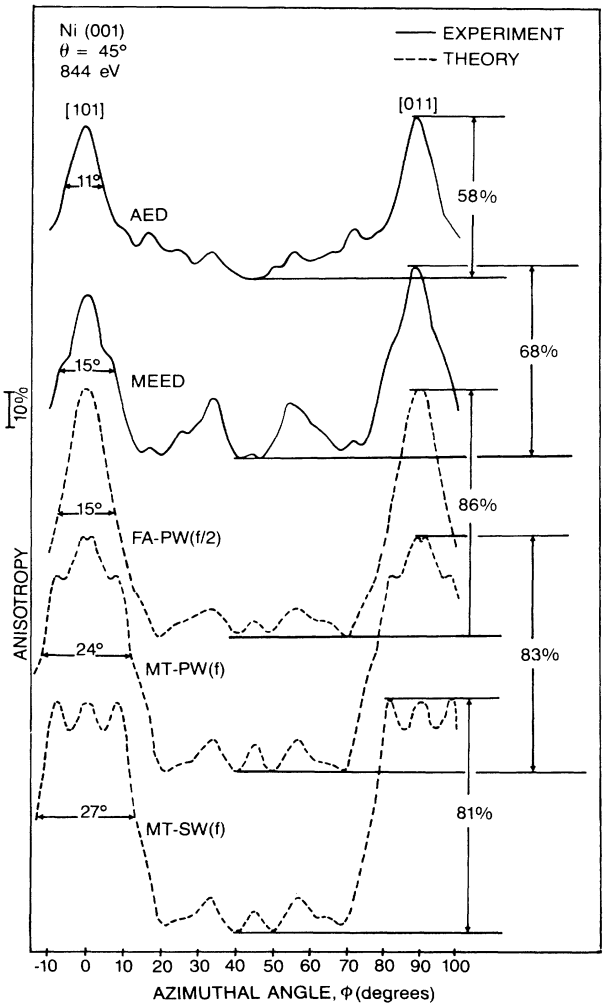

FIG. 3. AED, MEED, and calculated azimuthal-angle intensity distributions for $\theta=45°$ at 844 eV for a Ni(001) surface. The calculated curves result from evaluation of Eq. (3) and employ scattering factors based on plane waves interacting with a free-atom scattering potential (FA-PW), plane waves scattering from a muffin-tin potential (MT-PW), and spherical waves interacting with a muffin-tin potential (MT-SW). The FA-PW scattering strengths have been reduced by a factor of 2 to compensate for neglect of curved-wave effects and multiple scattering, whereas the MT-PW and MT-SW factors have not been.

widths and shapes of diffraction features along [101] and [011] are better accounted for with the FA-PW method. Therefore, it seems best to keep using empirically reduced FA-PW scattering factors in AED-MEED calculations rather than the more rigorous MT-PW or MT-SW factors. This apparently contradictory result may stem from deviations in angular momentum character of the emitted Auger and backscattered incident wave from the assumed s-wave character.

Returning to Fig. 1, we present plots of Eq. (1) in which FA-PW scattering factors reduced by a factor of 2 have been used to accompany the experimental data for Ni(001) and Cu(001). For each calculation we have examined the relative contributions of $I_{\text{in}}^{(l)}(\mathbf{k})$ and $I_{\text{out}}^{(l)}(\mathbf{k}')$ and have found that $I_{\text{in}}^{(l)}(\mathbf{k})$ changes very little with ϕ for $\theta=45°$. Therefore, the theoretical plots shown in Fig. 1 are essentially entirely due to scattering of the outgoing electron. In cases where the MEED and AED fine structure differ, the calculated angular distributions are more closely matched to the AED scans than to the MEED scans. For instance, at 707 and 772 eV, the dip at $\phi=45°$ seen in the AED profile is well reproduced by theory, and the peak seen in the MEED scan at $\phi=45°$ is not predicted. Similarly, the additional fine structures seen in the MEED scan at 1410 eV are not predicted by theory, whereas the match of theory to the XPD scan is excellent. Therefore, we conclude that the differences in fine structure between MEED and AED or XPD scans are *not* accounted for by modifying theory to include incoming beam diffraction in a simple way, as we have done here, even for this geometry in which changes in incident beam scattering with angle should be minimal. We now extend the analysis to angular scans in which incident beam channeling is expected to vary significantly with angle.

In Fig. 4 we show experimental and theoretical AED and MEED results for a polar scan in the (010) azimuthal plane for Ni(001). The theoretical calculation accompanying the AED scan includes only outgoing electron diffraction (hereafter referred to as SD for single diffraction) while that for the MEED scan separates outgoing electron scattering in the absence of incoming beam scattering (SD) from the predictions of Eq. (1) (hereafter referred to as DD for double diffraction). Agreement between SD theory and experiment is quite good in the case of AED. The MEED SD calculation (which is identical to the AED calculation, but with a kinetic energy of 1000 eV rather than 844 eV) is also in very good agreement with the MEED scan. However, inclusion of incident beam diffraction (DD) somewhat reduces agreement with experiment. The theoretical (DD) [101] diffraction feature (at $\theta=45°$) is made asymmetric as a result of strong forward scattering of the incident beam along [001] at $\theta=48°$ and is closer in appearance to the experimental peak than that generated by SD theory. However, the peak near $\theta=90°$ is shifted to higher polar angle than would otherwise occur and is highly asymmetric because of strong coupling of the incident beam to [101] at $\theta=93°$.

In Fig. 5 we show 1000-eV elastic peak intensities versus azimuthal angle at polar angles of $\theta=10°$, 15°, 18.4°, and 35.3° along with SD and DD calculated angular distributions. The first two scans do not encompass any low-index directions, while the scan at $\theta=18.4°$ includes [301] at $\phi=0°$ and [031] at 90° and the scan at $\theta=35.5°$ takes in [111] at $\phi=45°$. In general, it is seen from Fig. 5 that the inclusion of outgoing beam diffraction (DD) does not significantly alter the appearance of calculated angular distributions relative to those calculated within the SD approximation. The primary effect is a change in the relative intensities of the various diffraction features, the most noteworthy being the features at $\phi=20°$ and 70° in the scan at $\theta=10°$. The SD model predicts features which are much larger than those we observe or those predicted by DD theory. Overall, however, agreement between experiment and theory is essentially the same for the two models and is reasonably good at all polar angles. Most fine structure is accounted for and the predicted peak positions are in good agreement with experiment. It is clear from Fig. 5 that the inclusion of incoming beam diffraction does not significantly increase the level of agreement with experiment relative to SD theory.

There are three potential reasons why DD theory does not more accurately predict MEED angular distributions than does SD theory. The first is the neglect of the phase relationship between incoming and outgoing beams. This approximation greatly simplifies the calculation by allowing the problem to be broken down into two independent kinematical scattering parts and by allowing us to sum incoherently over backscatterers in Eq. (1). However, such an approximation may be too crude

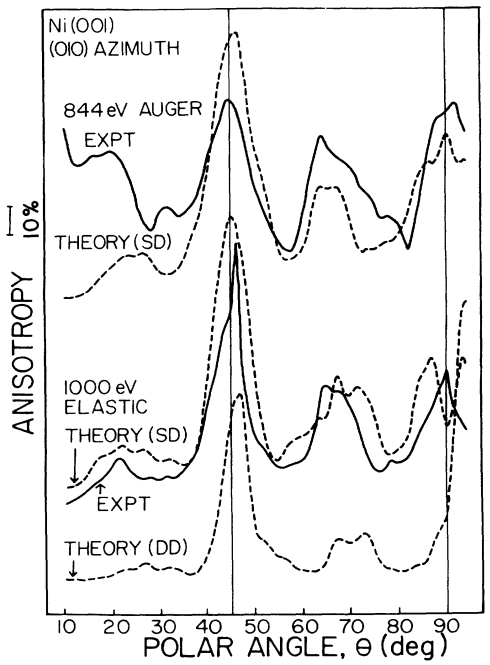

FIG. 4. Experimental and calculated polar profiles of AED and MEED intensities for Ni(001) in the (010) azimuth using Auger electrons of 844 eV and elastically scattered electrons of 1000 eV. The MEED calculation was performed with and without the inclusion of incident beam diffraction. The former is referred to as DD (for double diffraction) and the latter is referred to as SD (single diffraction).

for a fully quantitative theory of MEED phenomena.

A second possible reason for the failure of DD theory to more accurately predict experiment is the assumption that forward-scattered incoming waves can be approximated by their asymptotic spherical forms when they reach the lth backscatterer. Over this short range, the forward-scattered wave from the kth atom is rigorously expressed as

$$\Psi_k(\theta_k,r_k)=\sum_l (2l+1)\sin\delta_l \exp(i\delta_l) \times P_l(\cos\theta_k) i^{l+1} h_l^{(1)}(|k|r_k) , \quad (5)$$

where δ_l is the scattering phase shift for a partial wave with angular momentum l, $P_l(\cos\theta)$ is a Legendre polynomial of order l, and $h_l^{(1)}$ is a spherical Hankel function of the first kind. In the limit of $r_k \to \infty$, Eq. (4) reduces to

$$\Psi_k(\theta_k,r_k)=\left[\frac{1}{|k|}\sum_l (2l+1)\sin\delta_l \exp(i\delta_l)P_l(\cos\theta_k)\right] \times \left[\frac{1}{r}\exp(i|k|r_k)\right] \quad (6)$$

$$=\frac{f_k(\theta_k)}{r_k}\exp(i|k|r_k) . \quad (7)$$

This asymptotic form is simply a spherical wave centered on the kth scatterer which is modulated by a strongly forward-peaked complex scattering factor $f_k(\theta_k)$. The behavior of Eq. (5) a few angstroms away from the kth

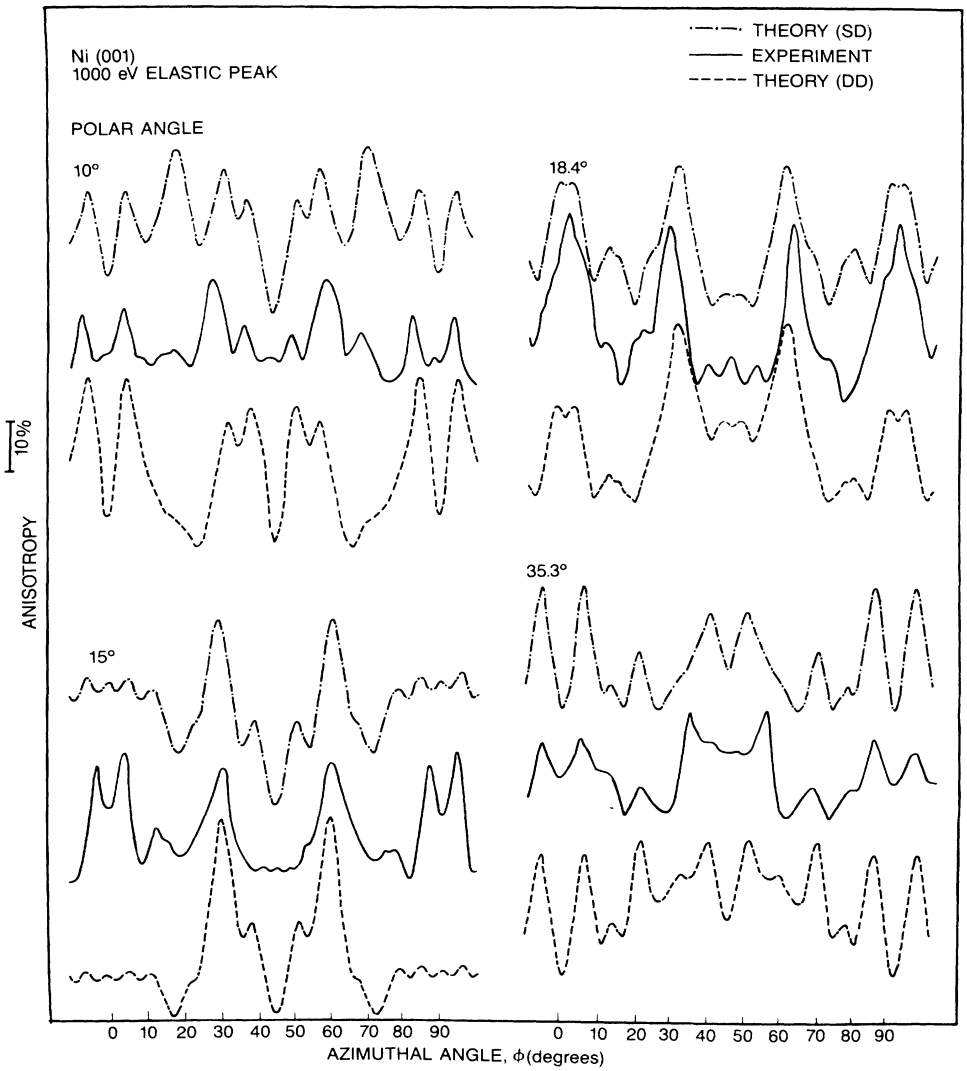

FIG. 5. Experimental MEED azimuthal-angle distributions along with related theoretical calculations at a variety of polar angles for Ni(001). For each polar angle, calculations have been performed with and without the inclusion of incident beam diffraction.

scatterer in the presence of other such scattered waves is very difficult to predict short of its inclusion in Eq. (2).

A third possible explanation of the failure of Eq. (2) to correctly describe incident beam diffraction is the neglect of multiple forward scattering, which tends to reduce forward focusing relative to the kinematical approximation by redirecting flux away from the incident direction. The overall effect is to reduce the kinematical anisotropies by filling in the regions between forward-scattering peaks as flux is deflected from the forward-focusing direction.[14] In light of the rather good agreement between MEED scans and the simpler and less time-consuming SD theory (indicating the relative unimportance of incoming beam diffraction), we have chosen not to attempt the aforementioned improvements to the DD theory.

In Fig. 6 we compare azimuthal MEED scans from the pseudomorphic interface formed by growing 12 Å of Cu on Ni(001) to SD calculations. The lattice constant normal to the interface was determined by MEED polar scans (3.75 Å) and was used for the pseudomorphic Cu overlayer calculations.[2] Comparing these experimental and theoretical angular distributions with those for Ni(001) in Fig. 5, it is clear that the tetragonal distortion does not significantly alter diffraction features in the stressed overlayer relative to those of the bulk substrate. All peaks observed in the Ni(001) scans are also seen in the 12-Å Cu/Ni(001) profiles, with little or no change in position. Only the relative intensities are modified, and these changes are rather small. Thus, it appears that such angular scans are not particularly sensitive to changes in lattice dimensions brought about by elastic strain. Shifts in the [101] peak position along the polar direction do track with tetragonal distortion and are quite straightforward to interpret. Such shifts should prove useful in a variety of overlayer studies.

In summary, we have compared the angular distributions associated with medium-energy elastically backscattered electrons and angular scans of high-energy Auger electrons and x-ray photoelectrons. The comparisons have been performed for bulk Ni(001) and Cu(001) samples. In general, we find that the three different experiments yield extremely similar results, indicating that the observed intensity anisotropies are governed largely by the scattering and subsequent interference of *outgoing* (or backscattered) electrons. Incident beam diffraction appears to play a relatively minor role. Experimental results are well reproduced by a simple kinematical scattering formalism in which only outgoing beam diffraction is treated. Inclusion of incoming beam scattering in a manner analogous to the way outgoing beam scattering is treated does not particularly improve the level of agreement between theory and experiment. Scattering factors involving free-atom and muffin-tin potentials have been compared, as have factors assuming an incident plane wave and those corrected for curved-wave effects. Although unmodified scattering factors calculated from a muffin-tin potential produce nearly the same level of forward-scattering intensities as do free-atom factors which have been empirically reduced, the former produce diffraction peaks which are considerably broader and of a more complex structure than either the latter or experiment. The addition of a curved-wave correction enhances fine structure on forward-scattering peaks, but this fine structure is not seen in experiment. Azimuthal profiles are not nearly as sensitive as polar profiles to tetragonal distortions associated with pseudomorphic overlayer growth. As reported earlier,[1,2] shifts in the polar angle at which the diffraction features associated with close-packed low-index directions in the overlayer maximize are a good indication of elastic distortion normal to the interface and enable strain determination in this direction with a pre-

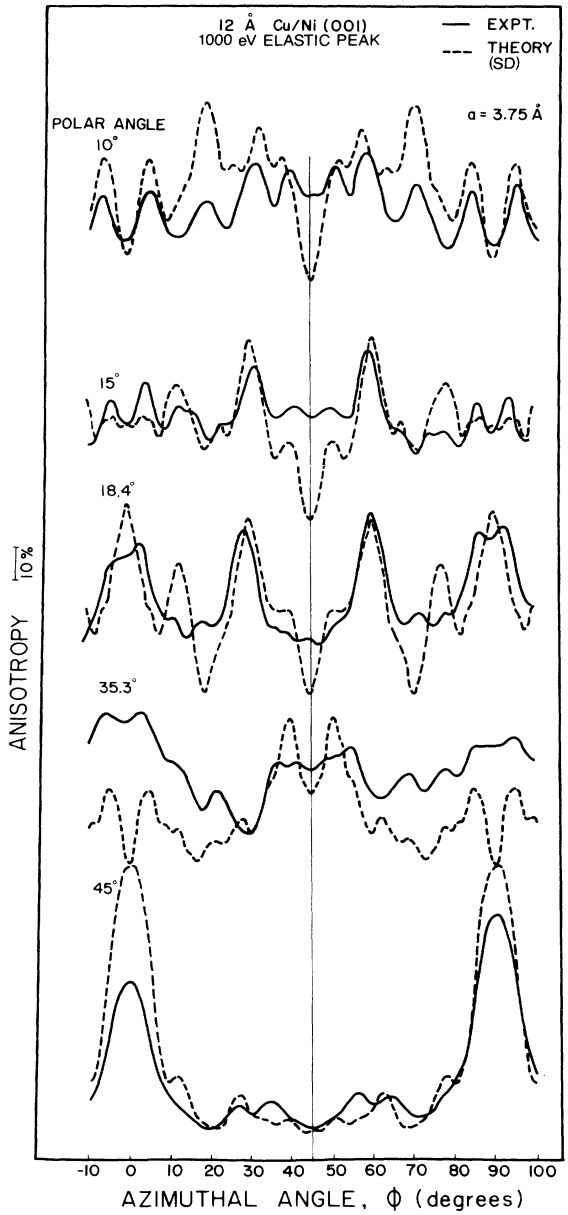

FIG. 6. Experimental MEED results and single-diffraction (SD) calculations for pseudomorphic Cu on Ni(001). The lattice constant normal to the interface used in the Cu/Ni calculations was obtained from polar-angle distributions of MEED intensity for this system (see Ref. 2).

cision of better than ±0.05 Å.

This work was supported by the National Science Foundation under NSF DMR-86-10837. Scattering calculations were performed on a CRAY-2 made possible by a grant from the Minnesota Supercomputer Institute. Stimulating interactions with C. S. Fadley are gratefully acknowledged.

---

*Present address: Boeing Electronics High Technology Center, P.O. 24969, MS9Z-80, Seattle, WA 98124-6269.

[1]S. A. Chambers, H. W. Chen, I. M. Vitomirov, S. B. Anderson, and J. H. Weaver, Phys. Rev. B **33**, 8810 (1986).

[2]S. A. Chambers, I. M. Vitomirov, S. B. Anderson, and J. H. Weaver, Phys. Rev. B **35**, 2490 (1987).

[3]C. S. Fadley in *Progress in Surface Science*, edited by S. G. Davison (Pergamon, New York, 1984), Vol. 16, p. 275.

[4]R. Trehan and C. S. Fadley, Phys. Rev. B **34**, 6784 (1986).

[5]S. A. Chambers, S. B. Anderson, H. W. Chen, and J. H. Weaver, Phys. Rev. B **34**, 913 (1986).

[6]S. A. Chambers, H. W. Chen, S. B. Anderson, and J. H. Weaver, Phys. Rev. B **34**, 3055 (1986).

[7]The extent of forward focusing increases with increasing kinetic energy. See, for example, Fig. 35 in Ref. 3.

[8]M. Fink and J. Ingram, At. Data **4**, 129 (1972).

[9]D. Gregory and M. Fink, At. Data Nucl. Data Tables **14**, 39 (1974).

[10]M. Sagurton, E. L. Bullock, R. Saiki, A. Kaduwela, C. R. Brundle, C. S. Fadley, and J. J. Rehr, Phys. Rev. B **33**, 2207 (1986).

[11]J. J. Barton and D. A. Shirley, Phys. Rev. B **32**, 1892 (1985).

[12]J. J. Rehr, R. C. Albers, C. R. Natoli, and E. A. Stern, Phys. Rev. B **34**, 4350 (1986).

[13]MUFPOT, originally developed by J. B. Pendry, was generously supplied to us by C. S. Fadley and co-workers.

[14]S. Y. Tong, H. C. Poon, and D. R. Snider, Phys. Rev. B **32**, 2096 (1985).